Microfluidics and Nanofluidics (2019) 23:115
https://doi.org/10.1007/s10404-019-2282-2

RESEARCH PAPER

Autonomous cell sorting using self-secreted macromolecules

Min Jung Kim[1] · **Jae Ryoun Youn**[1] · **Young Seok Song**[2]

Received: 1 May 2019 / Accepted: 10 September 2019 / Published online: 21 September 2019

Abstract

Much effort has been made to manipulate cells for many biomedical and environmental applications. However, controlling cells in efficient and sustainable ways is still an essential task to achieve in both science and engineering fields. Here, we introduced a strategic approach in which cells are autonomously sorted and separated in a fluidic system. We employed 'self-secreted macromolecules' from microalgae in the microfluidic devices and examined their various properties. The cell manipulation was determined depending on the intrinsic properties of the self-secreted biomolecules. The macromolecules self-produced by green algae allowed the size-based separation of cells. This self-sorting system would enable the design and fabrication of new types of biosystems such as bioreactors and pharmaceutical devices.

Graphic abstract

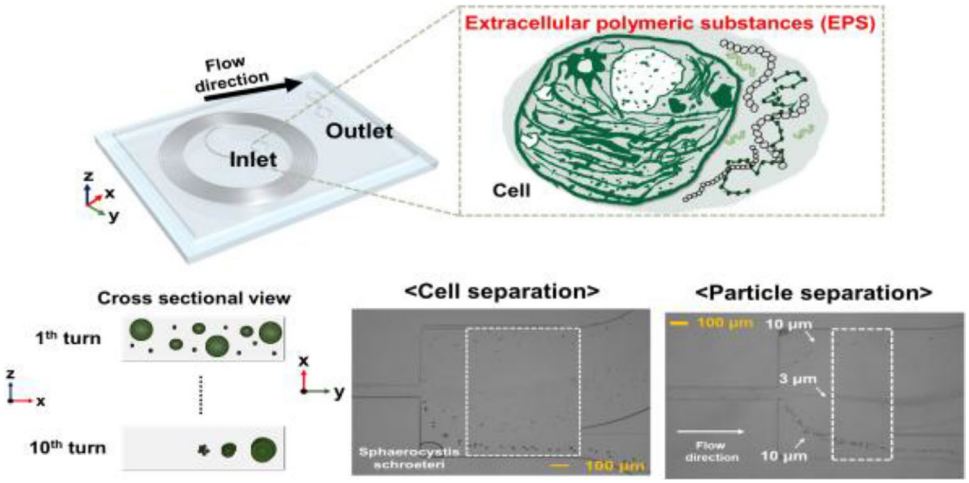

Keywords Extracellular polymeric substance (EPS) · Microalgae · Microfluidics · Cell manipulation

1 Introduction

'Self-secreted materials' from microorganisms, the so-called extracellular polymeric substances (EPSs) are abundant biosynthetic macromolecules which generate a protective layer of cells against external environment (Donlan 2002; Roberts 1996; Whitfield and Valvano 1993). Most notably, the biomacromolecules constructing three-dimensional network structures surrounding cells determine the structural integrity of biofilms (Flemming et al. 2007). The cells interact with their own EPSs and EPSs secreted by other cells (Hay 2013).

Electronic supplementary material The online version of this article (https://doi.org/10.1007/s10404-019-2282-2) contains supplementary material, which is available to authorized users.

✉ Jae Ryoun Youn
jaeryoun@snu.ac.kr

✉ Young Seok Song
ysong@dankook.ac.kr

[1] Department of Materials Science and Engineering, Research Institute of Advanced Materials (RIAM), Seoul National University, Seoul 08826, South Korea

[2] Department of Fiber System Engineering, Dankook University, Gyeonggi-do 16890, South Korea

The EPSs allow intense interactions between the cells, such as cell–cell communication and formation of synergistic microconsortia. On the other hand, microalgae produce EPSs according to their microbial metabolism determined by the environmental conditions. Consequently, the molecular composition of the EPSs is influenced by various factors, such as species, salinity, temperature, pH, and so on (De Philippis et al. 1991; Liu and Fang 2003; Xiao and Zheng 2016). The bio-macromolecules are composed of numerous polysaccharides, proteins, and e-DNAs, which contribute to the structure and function of EPSs. Physicochemical forces associated with the interaction between these molecules include the van der Waals forces, electrostatic interactions, and hydrogen bond (Mayer et al. 1999). Since exopolysaccharides with linear or branched long molecules have the highest content among the EPS components (Flemming and Wingender 2010), they can react with not only themselves but also other components such as DNA and proteins (glycoprotein molecules) due to the surface charge of polysaccharide (Sutherland 2001). In this sense, the EPSs can act as a non-permanent viscoelastic physical gel where chemical cross-linking mechanisms are excluded (Körstgens et al. 2001). In contrast to chemically induced cross-linking processes, it can be deformed by small perturbative forces (Wloka et al. 2004) such as hydrodynamic force. Under pressure driven flow, the length scales of macromolecules change dynamically as they stretch and tumble (Kim et al. 2012).

Photosynthetic microorganisms (e.g., microalgae, cyanobacteria, etc.) are well-known biological sources that are capable of producing a tremendous amount of EPSs. The microalgal EPSs have been studied for their potentials as natural resources for various applications (More et al. 2014; Xiao and Zheng 2016) such as biomass (Hossain et al. 2008) and electrical energy (Bombelli et al. 2012; McCormick et al. 2011). Thus, it is of a great importance to understand fundamentals of EPSs for various potential applications.

In the current study, we extracted abundant biosynthetic macromolecules from microalgae and investigated the strong elastic effect of EPSs on the particle migration in a microfluidic device. We demonstrated autonomous cell-sorting phenomenon adopting the biosynthetic macromolecules secreted by algae. In addition, enhanced particle separation was achieved using a spiral channel. S*phaerocystis schroeteri* with different size distributions was employed for the cell separation. It was found that the intrinsic properties (i.e., viscoelastic feature) of EPSs can be utilized for self-sorting and -separation of cells.

2 Materials and methods

2.1 Solution preparation

Fresh water microalgae, *Chlorella vulgaris* (AG10052) and S*phaerocystis schroeteri* (AG10007) strains were purchased from Korean Collection for Type Culture (KCTC), Korea. EPSs were extracted from *Chlorella vulgaris* which was cultivated in the BG11 medium (C3061, Sigma Aldrich) for 3 months before usage. To harvest the EPSs from microalgae, the disodium ethylenediaminetetraacetic acid (EDTA) method (Flemming et al. 2007; Liu and Fang 2002) was chosen. Biofilms were mixed with EDTA 2% (15105, Daejung Chemicals) and stored at 4 °C for 3 h. Subsequently, the sample was centrifuged at 3900 rpm and 25 °C for 20 min. Finally, the extracted EPSs were purified with a 0.2-μm membrane (C020A047A, Advantec MFS Inc., USA). *Sphaerocystis schroeteri* was cultivated in BG11 for 14 days before use. Morphology of *Sphaerocystis schroeteri* was examined with an inverted optical microscope (IX53, Olympus).

Three kinds of fluorescent polystyrene particles with sizes of 3 μm (79166, Sigma Aldrich), 6.27 μm (FP-6056, Spherotech), and 10.2 μm (C37259, Thermo Fisher Scientific) were suspended in the solution with a volume fraction of 0.1%.

2.2 Solution characterization

The sample was characterized in various ways (Kim et al. 2018). The total amount of extracted EPSs was estimated by measuring the weight of solids after lyophilization. The EPSs were characterized through the following chemical, structural, and rheological analyses:

1. Chemical analysis: the composition of the EPSs was analyzed using the following colorimetric methods, which employ the phenol–sulfuric acid method (DuBois et al. 1956), the Pierce® BCA protein assay (Thermo scientific, Rockford, IL, USA), and Nano-200 Nucleic Acid Analyzer (MEDCLUB, Tainan, Taiwan). The chemical structure of EPSs was investigated through Fourier transform infrared spectroscopy (FT-IR) analysis (Nicolet iS50, Thermo Fisher, Madison, USA). Solid samples were prepared via the lyophilization of aqueous solution. The degree of the cell destruction in EPSs was examined using a UV–Vis spectrometer (V-770, JASCO, Japan).
2. Structural analysis: The morphology of the biofilms was characterized using field emission scanning electron microscopy (FE-SEM; JSM-7600F, JEOL Ltd., Japan). Before the observation of biofilms, the biofilms were freeze-dried and mounted on a copper stub using an

adhesive carbon tape. Atomic force microscopy (AFM, NX-10, Park Systems) was used to observe the topographic image of exopolysaccharides. The molecules are spread on freshly cleaved mica substrate (a hydrophilic aluminosilicate mineral).

3. Rheological analysis: rheological properties were measured using a stress-controlled rheometer (Discovery HR-3, TA Instruments, New Castle, USA) with a 60-mm diameter parallel plate. The steady-state shear rates were applied in the range of 0.1 through 1000 1/s, and the angular frequency range was 1–100 rad/s. All the shear viscosity data were fitted successfully by the Carreau–Yasuda model and allowed the estimation of elasticity of the samples. The cross-over point between the loss modulus and the storage modulus gives the average relaxation time for EPSs assuming the Maxwell model described by $G'(\omega) = \eta\lambda\omega^2/\left(1+\lambda^2\omega^2\right)$ and $G''(\omega) = \eta\omega/\left(1+\lambda^2\omega^2\right)$, where η is the viscosity, ω is the angular frequency, and λ is the total average relaxation time. According to the classical Zimm's polymer theory, the relaxation time of semi-flexible polymer in good solvent depends on the coil size (Doi and Edwards 1988): $\lambda_z = F\frac{[\eta]M_w\eta_s}{N_A K_B T} \approx \frac{\eta_s R_g^3}{K_B T}$, where $[\eta]$ is the intrinsic viscosity of the solution, M_w is the polymer molecular weight, η_s is the viscosity of the solvent, N_A is Avogadro's number, K_B is the Boltzmann's constant, T is the absolute temperature, and R_g is the radius of gyration for semi-flexible polymer. $R_g \sim L^{\frac{3}{5}}\left(l_p d\right)^{\frac{1}{5}}$ is determined by the contour length (L), the persistence length $\left(l_p\right)$ reflecting the chain stiffness, and the effective polymer diameter (d) (Rubinstein and Colby 2003). That is, the total average relaxation time is determined by the linear combination of the chemical components constituting the EPSs and the structural information of the EPSs.

2.3 Microchip fabrication and imaging

Experiments were carried out in a straight microchannel with square-shaped cross-section and a spiral microchannel with rectangular-shaped cross-section, which were made of poly(dimethylsiloxane) (PDMS, Sylgard 184, Dow Corning) replica. The microfluidic devices were fabricated using a standard soft lithography technique. The base and curing agent of PDMS (10:1) were mixed and degassed for 40 min. The mixture was poured onto the SU-8 photoresist mold and cured in an oven at 70 °C for 12 h. The PDMS replica was bonded onto the glass after oxygen plasma treatment. Then, the devices were placed on a hotplate at 120 °C for 20 min to increase bonding strength. The dimension of the straight square microchannel was 50 μm × 50 μm × 5 cm (Fig. 1a). The spiral channel had ten loops, and its width and height

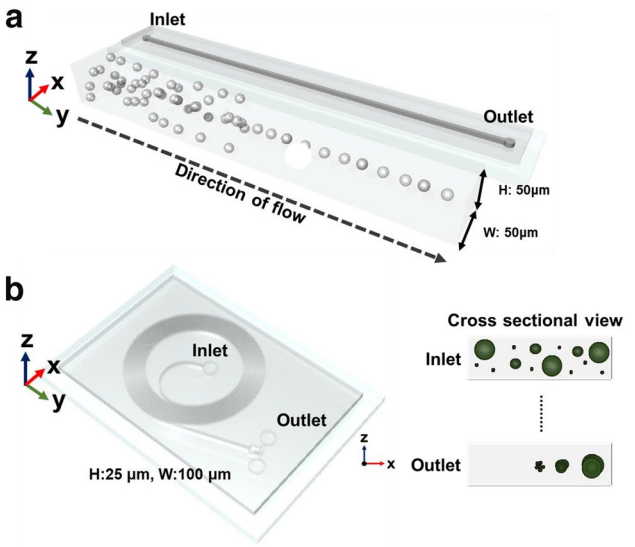

Fig. 1 Schematic diagram of the microfluidic chips used in this study. **a** Schematic illustration for Elasto-inertial particle focusing under the EPS solution in a square channel. As the distance from the inlet increases, the Elasto-inertial particle focusing within the channel appears as a line. **b** Schematic illustration for Dean-coupled Elasto-inertial particle focusing under the EPSs solution in a spiral channel. In a confined microchannel, different sized particles show different equilibrium positions at an outlet due to elastic force and Dean drag force

were 100 and 25 μm, respectively. The initial radius of curvature was 9.5 mm, and the total arc-length was approximately 50 cm (Fig. 1b). The spiral microfluidic channels were designed and constructed to figure out the elastic force and Dean drag force for particle migration according to the size of particles (Lee et al. 2013).

Particle dynamics was observed using an inverted optical microscope (IX53, Olympus), and the images were acquired with a high-speed fluorescence camera (AcquCAM 23G, JNOpTIC co., Ltd) using an image software package (JNOPTIC Capture 2.4). The ImageJ (NIH) 1.52a software was used for image processing to determine the particle distribution in the microchannel. The images were stacked in the z direction using either the 'standard deviation' or 'min intensity' options. The size of the cells used in the microchannel experiments was obtained via the image processing. It was assumed that the cell has a spherical shape and the cell diameter was rounded off to the first decimal point.

2.4 Numerical simulation

Finite element simulation was carried out to analyze the particle focusing behavior by harnessing the Oldroyd-B model in the straight microchannel. For simulation, the steady-state momentum equation is expressed as $Re(u\cdot\nabla)u = \nabla\cdot\left(-pI + \left(\eta_s/\eta\right)\left[\nabla u + (\nabla u)^T\right] + T\right)$,

and the extra stress contribution becomes $T + Wi_T^{\nabla} = \left(\eta_p/\eta\right)\left[\nabla u + (\nabla u)^T\right]$. Here, *Re* and *Wi* are the Reynolds number and the Weissenberg number, respectively. η_s is the relative solvent viscosity, η_p is the relative polymer viscosity, and the total viscosity, $\eta = \eta_s + \eta_p$. $\overset{\nabla}{T}$ is the upper convected derivative of the stress tensor expressed as $\overset{\nabla}{T} = \partial T/\partial t + (u \cdot \nabla)T - \left[(\nabla u) \cdot T + T \cdot (\nabla u)^T\right]$.

3 Results and discussion

In most natural environments, sessile microbes live in an aggregated form secreting various biomaterials, such as biofilms (Wingender et al. 1999). In particular, photosynthetic microorganisms excrete a large quantity of biosynthetic macromolecules during photosynthesis. The self-secreted materials, i.e., EPSs are mainly composed of polysaccharides, proteins, and extracellular DNA (e-DNA) with weak physicochemical interactions. The EPSs can behave as a non-permanent viscoelastic physical gel.

3.1 Characterization of self-secreted biomaterials

To figure out physicochemical properties of the self-secreted biomaterials, various characteristics of the EPSs were examined. Through colorimetric analysis, the concentrations of polysaccharides, proteins, and DNA were evaluated as listed in Table 1. The major component of EPSs was polysaccharides, which accounted for 99% of the total mass. In other words, the ratio of protein/polysaccharide was very low (Liu and Fang 2003). The EPSs were analyzed using infrared spectrophotometry, and the result is shown in Fig. 2a. The spectrum displays clear absorption peaks at 1215, 1347, 1619, 3015, and 3392 cm^{-1}. The band at 1215 cm^{-1} was attributed to the C–N stretching vibration of the amino acids of proteins. The strong peak at 1619 cm^{-1} and 1347 cm^{-1} was related to the C=O symmetric and anti-symmetric stretching in the carboxylate (Deng et al. 2003) and/or stretching vibration of the amino acids of proteins (Zhou et al. 2016). The weak band at 3015 cm^{-1} corresponded to the $–CH_3$ stretching vibration of fatty acids. The broad peak at 3392 cm^{-1} was associated to –OH carbohydrates and/or –NH of proteins (Deng et al. 2003). These results confirmed the presence of the amino, hydroxyl, and carboxyl group in the extracted EPSs. UV–Vis analysis also confirmed that the cell destruction did not occur during the extraction process (Fig. 2b).

Table 1 Composition of the EPSs extracted using the EDTA method

Extraction method	Composition of EPSs (μg/ml)		
	Polysaccharide	Protein	e-DNA
EDTA method	73,400	469	274

In addition, the sample was observed using AFM to obtain the nanostructural information of polysaccharides with the highest proportion in the extracted EPSs. The topographical structures of exopolysaccharides are shown in Fig. 3a. The height of the fibril was under 1 nm corresponding to the dimension of a single molecular exopolysaccharide chain (Abu-Lail and Camesano 2003). The extracted exopolysaccharide molecules with a length of hundreds of nanometers possessed linear conformation, which resulted in shear-thinning behavior (Morris 1990). The globules indicated positively charged proteins (Svetličić et al. 2011). The EPSs form three-dimensional networks near cells providing mechanical stability of biofilms. The SEM images confirmed the role of the EPSs as a protective layer (Fig. 3b).

Rheological investigations about the EPSs were conducted. The shear viscosity of the EPSs was divided into two regions: zero-shear viscosity region and shear thinning region (Fig. 4a). The zero-shear viscosity of the EPSs was approximately 0.018 Pa s. The shear-thinning behavior of the EPSs was explained with help of the alignment of entangled molecules along the direction of applied shear flow (Smith et al. 1999). The particle migration is affected by both the shear force and inertial forces (Li et al. 2015; Song et al. 2016). Figure 4b shows the results of dynamic oscillatory shear tests. The storage and loss moduli increased with respect to the angular frequency. The intersection point

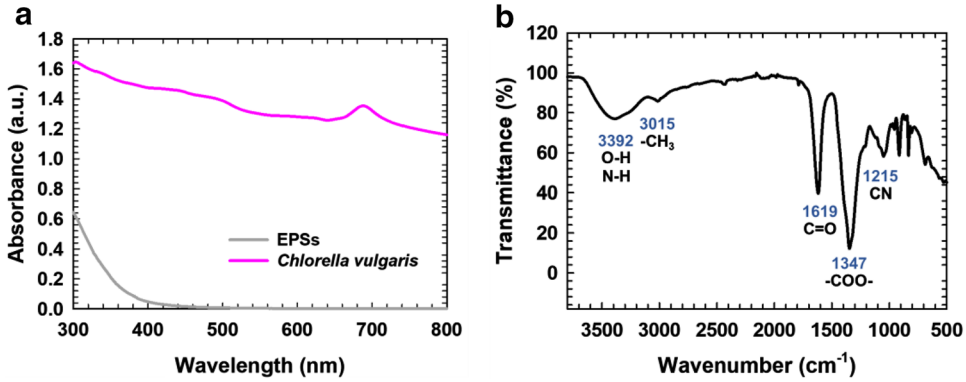

Fig. 2 Chemical characterization of EPSs. **a** FT-IR spectrum of the EPSs extracted from *Chlorella vulgaris*. **b** UV–Vis spectra of *Chlorella vulgaris* and EPSs

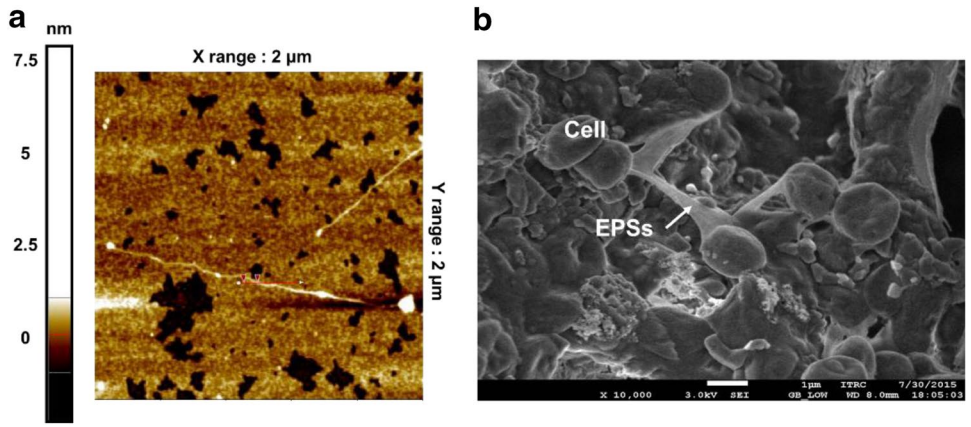

Fig. 3 Structural characterization of EPSs. **a** AFM image of exopolysaccharide of the EPSs. **b** SEM image of *Chlorella vulgaris* embedded in biofilm. The scale bar denotes 1 μm

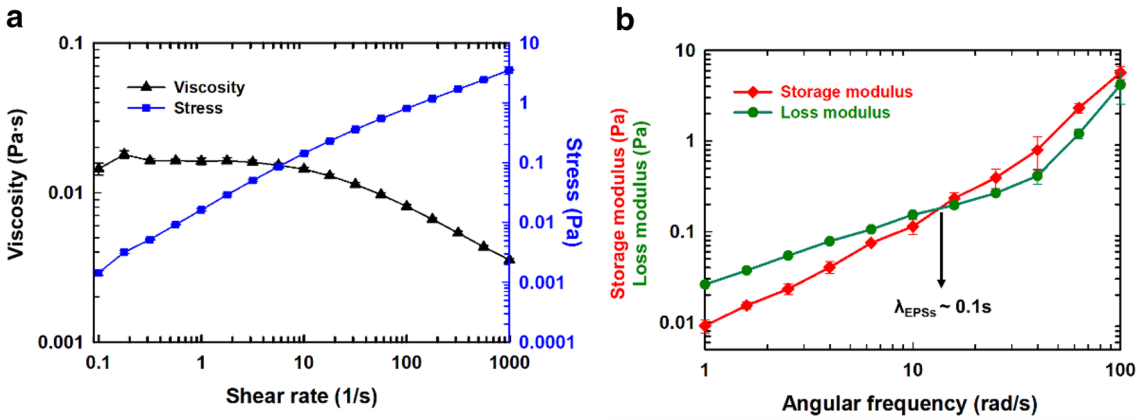

Fig. 4 Rheological characterization of EPSs. a Rheological properties of the EPSs as a function of the shear rate ranging from 0.1 to 1000 s^{-1}. **b** Storage modulus (G') and loss modulus (G'') as a function of the angular frequency

between the loss and the storage moduli characterized the average relaxation time with an order of 0.1 s. The elasticity of the sample could be evaluated using the Weissenberg number ($Wi \equiv \lambda\,\dot{\gamma}$), which is defined by the combination of the relaxation time (λ) and the strain rate of flow ($\dot{\gamma}$). The relaxation time was determined based on the linear combination of the relaxation times of the materials by following the proportion of each substance in the sample.

3.2 Particle manipulation

The elastic property of non-Newtonian fluid entails particle alignment along the centerline of a microchannel due to the non-uniform distribution of first normal stress difference (N_1) (Song et al. 2016). In other words, it is expected that the particle focusing along the centerline of a channel can occur because of the elastic property of the EPSs. We exploited an extraordinary particle focusing phenomenon in the EPS solution in pressure driven microflow. More specifically, migration of the fluorescent particles (diameter = 6.27 μm) within a straight square microchannel (length: 5 cm; width × height: 50 μm × 50 μm) was examined under a flow rate of 50 μl/h ($Re = 0.019$, $Wi = 22.2$). To demonstrate the lateral migration of particles at five different axial locations of the channel, overlaid fluorescent images were acquired (Fig. 5a). Figure 5b presents the probability density function determined across the channel width. Once randomly distributed particles were injected into the microchannel, they were significantly aligned along the channel centerline. This phenomenon is called the 'elasto-inertial particle focusing'. Thus, we identified that the EPSs composed of polysaccharide, protein and e-DNA could serve as a particle focusing driving matter.

Finite element simulation was carried out to provide further physical insight into the particle migration using the first normal stress difference (Fig. 6a). For most polymeric liquids, $|N_2|/N_1$ is smaller than 10. Therefore, the effect of N_2 can be ignored (Bird et al. 1987). The main force exerting on the particles is the elastic force ($\overrightarrow{F_E}$), which is scaled as $\overrightarrow{F_E} \approx D_P^3 \nabla N_1$. It is proportional to the particle diameter (D_p) and the gradient of the first normal stress difference (N_1). Since the normalized value of N_1 showed minimum values

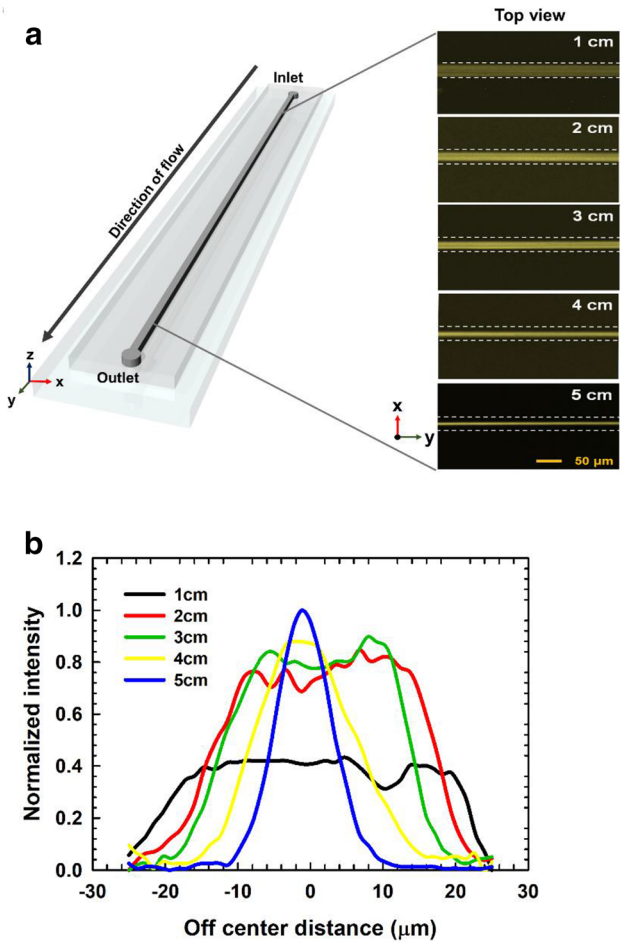

Fig. 5 Lateral particle migration in the EPS solution. **a** Particle focusing of 6.27-μm fluorescent PS particles. The hashed lines indicate the channel walls. A set of 50 images was overlaid to acquire the distribution of particles downstream from the inlet. The scale bar implies 50 μm. **b** Probability distribution function of the PS particles was observed 1 cm, 2 cm, 3 cm, 4 cm, and 5 cm downstream from the inlet. Both **a** and **b** were obtained at the flow rate of 50 μl/h

at four corners and at the center of the cross-section of the channel, particles tended to migrate the center and four corners. We also affirmed that the normalized first normal stress difference (N_1) shows the lowest values at the center of the cross-section ($x/L=0$), as shown in Fig. 6b.

Multiplex particle focusing was also examined with particles of 3 μm and 10 μm diameters in a spiral microchannel at a flow rate of 400 μl/h (Fig. 7). In a spiral microchannel, the equilibrium position of particles moving within the non-Newtonian medium is determined by the combination of the Dean drag force ($\overrightarrow{F_D} \approx \rho U^2 D_h^2 D_p/\gamma$) and the viscoelastic force ($\overrightarrow{F_E} \approx D_P^3 \nabla N_1$). Therefore, the equilibrium position of particles is determined by the particle size. According to the previous report (Lee et al. 2013), the normalized Dean force is related to the channel aspect ratio (γ) and the blockage ratio (D_p/D_h). Lee et al. (2013) showed that the Dean forces significantly increase with respect to the blockage ratio. We investigated the influence of particle size on the equilibrium position after ten turns. In Fig. 7a, the 3-μm particle had an equilibrium position at the centerline of the channel, indicating that the viscoelastic force dominated the Dean drag force. However, in the case of the 10-μm size particles, the lateral displacement of the equilibrium position was observed due to the Dean drag force (Fig. 7c). The probability distribution function for both particles indicated that the equilibrium positions were affected greatly by the particle size. In other words, as the number of turns increased, the larger particles were positioned closer to the outer channel wall. Therefore, the different sized particles could be separated and bifurcated at the outlet (Fig. 7e).

3.3 Autonomous cell sorting

For the separation of cells with a wide size distribution, *Sphaerocystis schroeteri*, a genus of green algae with 1–30 μm diameter was selected and employed. The cells with various sizes were injected into the spiral microchannel at a flow rate of 400 μl/h. It was observed in the first turn that the larger cells were located on the wall of the channel. The cells were

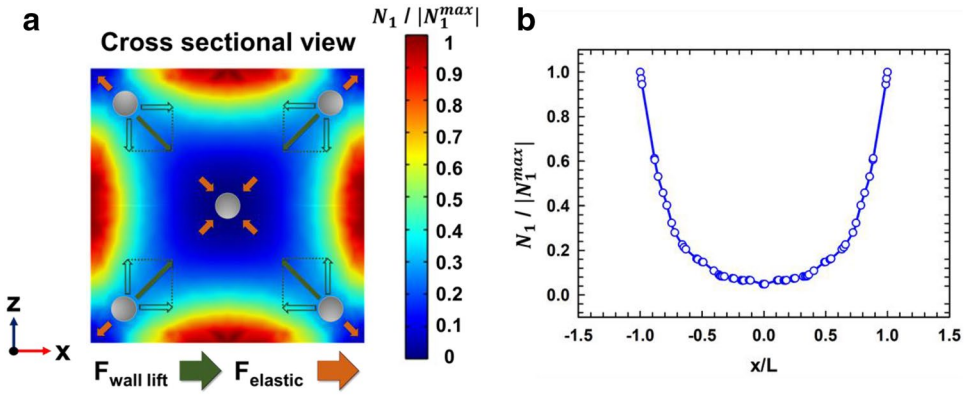

Fig. 6 Analysis of particle focusing phenomena. **a** Predicted distribution of the first normal stress difference (N_1) and schematic expression of forces exerted on a rigid particle under viscoelastic flows. **b** The value of the normalized first normal stress difference (N_1) shows symmetry at the cross-section of the channel

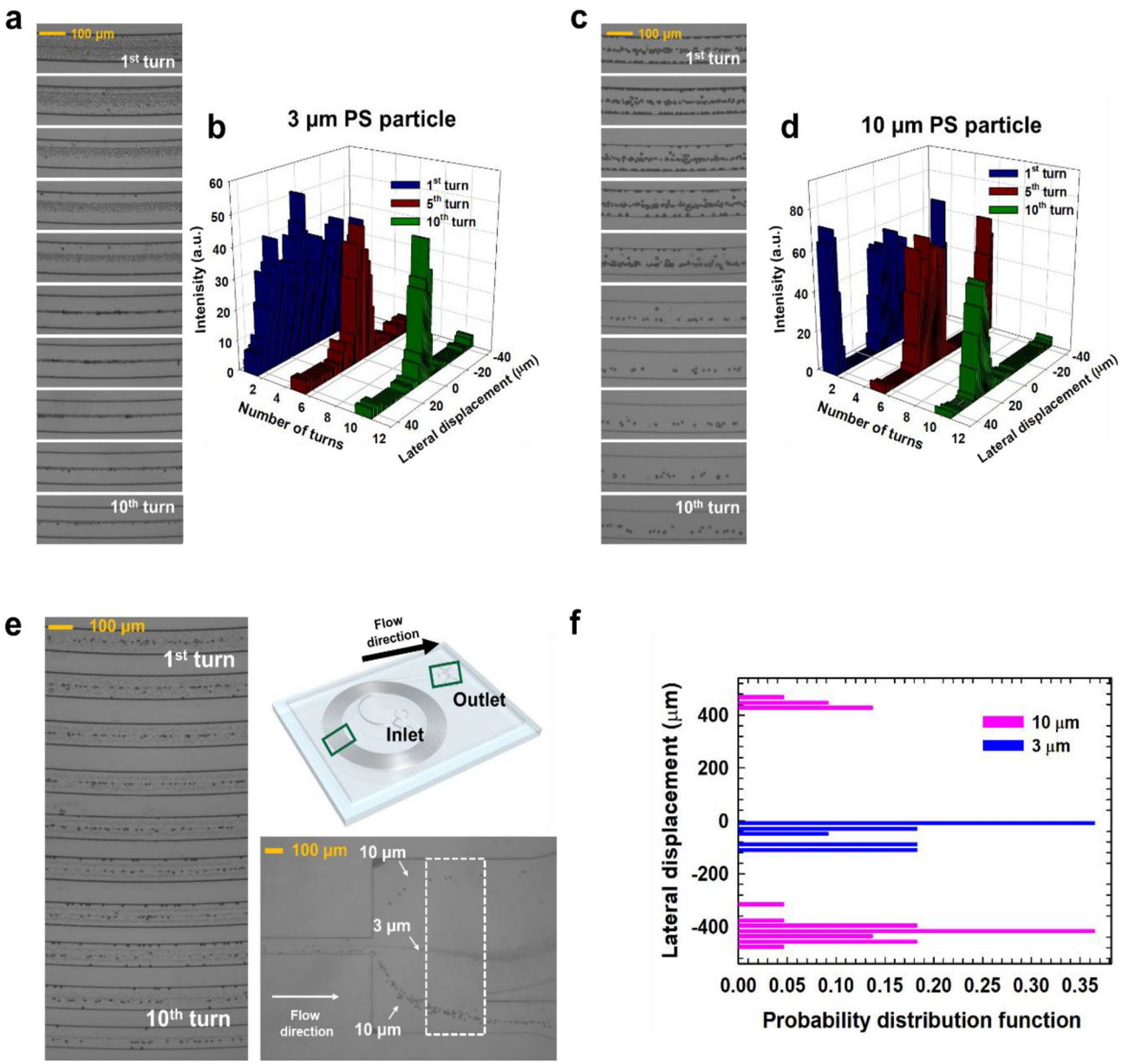

Fig. 7 Particle separation using the self-secreted biomaterials. Microscopic images for **a** the 3-μm PS particles and **c** the 10-μm PS particles in the EPSs solution with a flow rate of 400 μl/h ($Re = 0.122$, $Wi = 88.9$), constructed from sequences of high-speed microscopy images. Probability distribution functions for **b** the 3-μm PS particles and **d** the 10-μm PS particles after 1, 5 and 10 turns, showing particle focusing at the center and at the off-center, respectively. **e** Microscopic images illustrating the position and separation of the 3- and 10-μm PS particles at the outlet of the channel. **f** Probability distribution function of the 3- and 10-μm PS particles at the outlet

focused by the hydrodynamic force faster than rigid particles due to the deformability and shape of cells (Kim et al. 2018). The streak positions of the cells observed in the tenth turn indicated that multiplexing cell focusing was accomplished with respect to the size (Fig. 8a). The equilibrium position of the larger cell (> 16 μm) was situated at the outer side of the channel by the Dean Drag force. In addition, the equilibrium position was located at the middle or between the middle and the outside of the microchannel when diameter of the cells was smaller than 16 μm. Consequently, autonomous cell sorting was achieved using the self-secreted biomaterials, and the related video clip is available in the supplementary information (Movie S1). Indeed, this cell-focusing/sorting system is sustainable and efficient because the self-produced macromolecules are employed for the cell suspension. Probability distribution of the cells at the outlet is illustrated in Fig. 8b. The small cells were mostly distributed in area 3 (55.3%) due to the viscoelastic force. When the cells form a long cluster

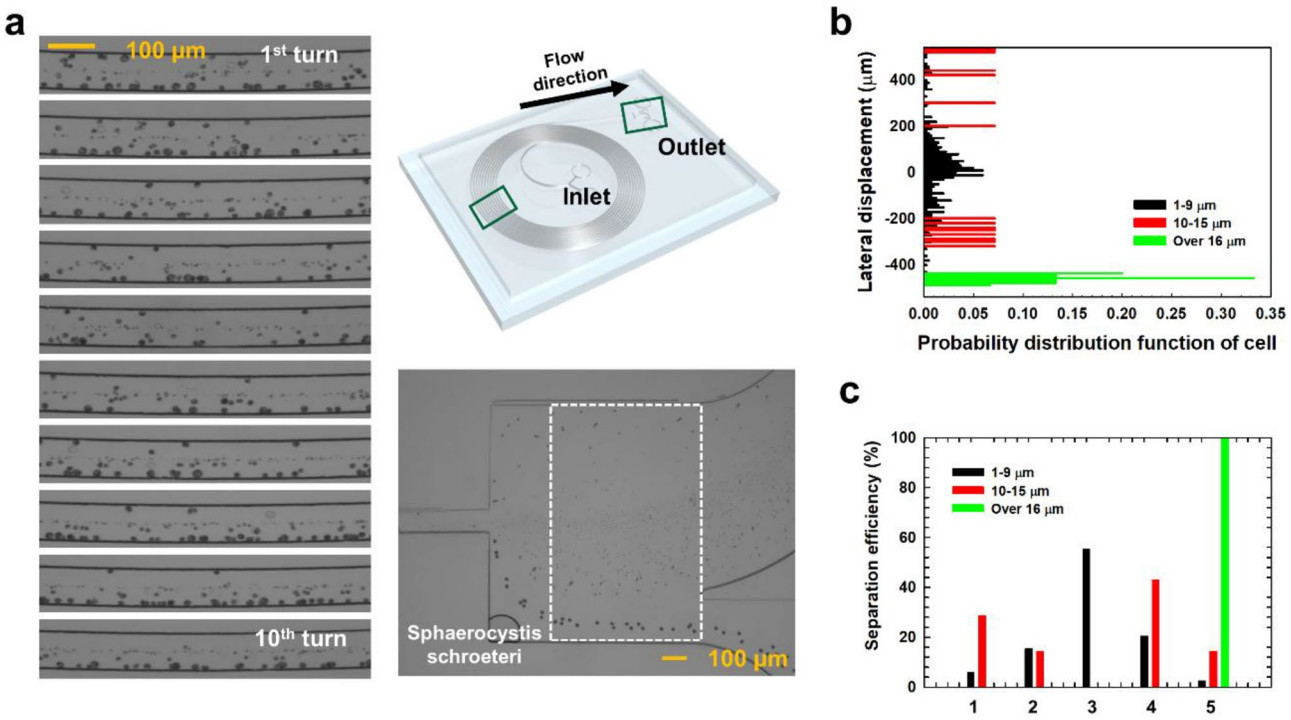

Fig. 8 Autonomous cell sorting using the self-secreted macromolecules. **a** Microscopic images of the cells in the EPS solution with a flow rate of 400 μl/h ($Re = 0.122$, $Wi = 88.9$), constructed from sequences of high-speed microscopy images. The superimposed images illustrate the distribution and position of the cells with different sizes in the channel. **b** Probability distribution function of the cells at the outlet of the channel. **c** Separation efficiency of the cells. The graph demonstrates the ratio of the cells moving to a specific area (area 1: 540–300 μm, area 2: 300–100 μm, area 3: 100 to −100 μm, area 4: −100 to −300 μm, and area 5: −300 to −540 μm)

(10–15 μm), they were mainly placed in area 1 (28.5%) or in area 4 (42.85%). When the cells have a diameter larger than 16 μm, they were all located in area 5. The proposed system has a limitation of separation cells in the range of 1–9 μm since the cells are deformable compared to the particles and strongly focus on the centerline of the channel. Our ongoing effort is to optimize the separating conditions of small-sized cells (1–9 μm) by considering the deformation of cells.

Live cells are deformable particles, which can lead to additional lift forces in contrast to rigid particles. The additional force originates from the flow disturbance due to the shape change of cells (Amini et al. 2014; Tam and Hyman 1973). In general, three dimensionless parameters can be used to characterize the relative deformation of a droplet: the Weber number, the Capillary number, and the internal-to-external viscosity ratio, as follows:

$$We = \frac{\rho U^2 a}{\sigma} \text{ (Inertial stress vs. surface tension)}, \quad (1)$$

$$Ca = \frac{\mu U a}{\sigma h} \text{ (Viscous stress vs. surface tension)}, \quad (2)$$

$$\lambda_d = \mu_d / \mu, \quad (3)$$

where a is the deformable particle diameter, and μ_d is the dynamic viscosity of fluid inside the deformable particle. The Weber number and the Capillary number characterize the relative deformation expected for a deformable particle (Hur et al. 2011; Mortazavi and Tryggvason 2000). The internal-to-external viscosity ratio is important parameter that provide deformation and drift of the deformable particle (Chan and Leal 1979; Doddi and Bagchi 2008; Hur et al. 2011; Magnaudet et al. 2003; Mortazavi and Tryggvason 2000). The lift force induced by the deformability is given by

$$\overrightarrow{F_{L,d}} \approx Ca \mu U a \left(\frac{a}{H}\right)^3 \left(\frac{d}{H}\right) f(\lambda_d), \quad (4)$$

where d is the distance between the deformable particle and the center of channel (Chan and Leal 1979). Here, $f(\lambda_d) = \frac{16\pi}{(\lambda_d+1)^3}\left[\frac{11\lambda_d+10}{140}\left(3\lambda_d^3 - \lambda_d + 8\right) + \frac{3}{14}\frac{19\lambda_d+16}{3\lambda_d+2}\left(2\lambda_d^2 - \lambda_d - 1\right)\right]$ (Chan and Leal 1979; Stan et al. 2013; Zhang 2015). When $\lambda_d < 1$ or $\lambda_d > 10$, the deformability-induced lift force is imposed towards the center of channel (Zhang 2015). That is, migration towards the channel wall was observed in the internal-to-external viscosity ratio ranging from 0.5 to 10 (Chan and Leal 1979; Hur et al. 2011; Magnaudet et al.

2003; Mortazavi and Tryggvason 2000). Green algae Prokaryotes such as *Lactococcus lactis* have a cellular viscosity of 6 mPa s (Cuecas et al. 2016), which implies that the viscosity ratio is 0.4. As a result, the cells strongly tend to move towards the centerline of channel due to the deformability-induced lift force. For this reason, the cells and PS particles have different range of sizes for separation.

4 Conclusions

We demonstrated autonomous cell sorting in a microfluidic device using the EPSs excreted by algae. Enhanced particle focusing and separation of rigid particles were also investigated with use of the self-secreted macromolecules. The extracted EPSs were examined through chemical, structural, and rheological analyses. The correlation between the viscoelastic properties of EPSs and the particle migration was explored. It was found that the EPSs prepared in this study could induce the multiplex focusing of particles with different sizes in the microfluidic device. This is attributed to the viscoelasticity of EPSs produced by microorganisms. It is expected that this study will provide a promising method to deal with cells for biomedical, pharmaceutical, and clinical applications.

Acknowledgements This work was supported by GRRC program of Gyeonggi Province (GRRC Dankook2016–B03). In addition, this research was supported by Basic Science Research Program through the National Research Foundation of Korea (NRF) funded by the Ministry of Education (2018R1D1A1B07049173) and by the Korea government (MSIT) (No. NRF-2018R1A5A1024127). Korea Institute for Advancement of Technology (KIAT) grant funded by the Korea Government (MOTIE) (P0002007, The Competency Development Program for Industry Specialist). The authors are grateful for the supports.

Compliance with ethical standards

Conflict of interest The authors declare the following competing financial interest(s).

References

Abu- Lail N, Camesano T (2003) Polysaccharide properties probed with atomic force microscopy. J Microsc 212:217–238

Amini H, Lee W, Di Carlo D (2014) Inertial microfluidic physics. Lab on a Chip 14:2739–2761

Bird RB, Armstrong RC, Hassager O (1987) Dynamics of polymeric liquids, volume 1: fluid mechanics. Wiley, New York

Bombelli P et al (2012) Surface morphology and surface energy of anode materials influence power outputs in a multi-channel mediatorless bio-photovoltaic (BPV) system. Phys Chem Chem Phys 14:12221–12229

Chan P-H, Leal L (1979) The motion of a deformable drop in a second-order fluid. J Fluid Mech 92:131–170

Cuecas A, Cruces J, Galisteo-López JF, Peng X, Gonzalez JM (2016) Cellular viscosity in prokaryotes and thermal stability of low molecular weight biomolecules. Biophys J 111:875–882

De Philippis R, Sili C, Tassinato G, Vincenzini M, Materassi R (1991) Effects of growth conditions on exopolysaccharide production by Cyanospira capsulata. Biores Technol 38:101–104

Deng S, Bai R, Hu X, Luo Q (2003) Characteristics of a bioflocculant produced by Bacillus mucilaginosus and its use in starch wastewater treatment. Appl Microbiol Biotechnol 60:588–593

Doddi SK, Bagchi P (2008) Lateral migration of a capsule in a plane Poiseuille flow in a channel. Int J Multiph Flow 34:966–986

Doi M, Edwards SF (1988) The theory of polymer dynamics, vol 73. Oxford University Press, Oxford

Donlan RM (2002) Biofilms: microbial life on surfaces. Emerg Infect Dis 8:881

DuBois M, Gilles KA, Hamilton JK, Rebers PT, Smith F (1956) Colorimetric method for determination of sugars and related substances. Anal Chem 28:350–356

Flemming H, Wingender J (2010) The biofilm matrix. Nat Rev Microbiol 8:623–633

Flemming HC, Neu TR, Wozniak DJ (2007) The EPS matrix: the "house of biofilm cells". J Bacteriol 189:7945–7947

Hay ED (2013) Cell biology of extracellular matrix, 2nd edn. Springer, New York

Hossain AS, Salleh A, Boyce AN, Chowdhury P, Naqiuddin M (2008) Biodiesel fuel production from algae as renewable energy. Am J Biochem Biotechnol 4:250–254

Hur SC, Henderson-MacLennan NK, McCabe ER, Di Carlo D (2011) Deformability-based cell classification and enrichment using inertial microfluidics. Lab Chip 11:912–920

Kim JY, Ahn SW, Lee SS, Kim JM (2012) Lateral migration and focusing of colloidal particles and DNA molecules under viscoelastic flow. Lab Chip 12:2807–2814

Kim MJ, Youn JR, Song YS (2018) Focusing manipulation of microalgae in a microfluidic device using self-produced macromolecules. Lab Chip 18:1017–1025

Körstgens V, Flemming H-C, Wingender J, Borchard W (2001) Uniaxial compression measurement device for investigation of the mechanical stability of biofilms. J Microbiol Methods 46:9–17

Lee DJ, Brenner H, Youn JR, Song YS (2013) Multiplex particle focusing via hydrodynamic force in viscoelastic fluids. Sci Rep 3:3258

Li G, McKinley GH, Ardekani AM (2015) Dynamics of particle migration in channel flow of viscoelastic fluids. J Fluid Mech 785:486–505

Liu H, Fang HH (2002) Extraction of extracellular polymeric substances (EPS) of sludges. J Biotechnol 95:249–256

Liu Y, Fang HH (2003) Influences of extracellular polymeric substances (EPS) on flocculation, settling, and dewatering of activated sludge. Crit Rev Environ Sci Technol. https://doi.org/10.1080/10643380390814479

Magnaudet J, Takagi S, Legendre D (2003) Drag, deformation and lateral migration of a buoyant drop moving near a wall. J Fluid Mech 476:115–157

Mayer C, Moritz R, Kirschner C, Borchard W, Maibaum R, Wingender J, Flemming H-C (1999) The role of intermolecular interactions: studies on model systems for bacterial biofilms. Int J Biol Macromol 26:3–16

McCormick AJ, Bombelli P, Scott AM, Philips AJ, Smith AG, Fisher AC, Howe CJ (2011) Photosynthetic biofilms in pure culture harness solar energy in a mediatorless bio-photovoltaic cell (BPV) system. Energy Environ Sci 4:4699–4709

More T, Yadav J, Yan S, Tyagi R, Surampalli R (2014) Extracellular polymeric substances of bacteria and their potential environmental applications. J Environ Manage 144:1–25

Morris ER (1990) Shear-thinning of 'random coil' polysaccharides: Characterisation by two parameters from a simple linear plot. Carbohydr Polym 13:85–96

Mortazavi S, Tryggvason G (2000) A numerical study of the motion of drops in Poiseuille flow. Part 1. Lateral migration of one drop. J Fluid Mech 411:325–350

Roberts IS (1996) The biochemistry and genetics of capsular polysaccharide production in bacteria. Annu Rev Microbiol 50:285–315

Rubinstein M, Colby RH (2003) Polymer physics, vol 23. Oxford University Press, New York

Smith DE, Babcock HP, Chu S (1999) Single-polymer dynamics in steady shear flow. Science 283:1724–1727

Song HY, Lee SH, Salehiyan R, Hyun K (2016) Relationship between particle focusing and dimensionless numbers in elasto-inertial focusing. Rheol Acta 55:889–900

Stan CA, Ellerbee AK, Guglielmini L, Stone HA, Whitesides GM (2013) The magnitude of lift forces acting on drops and bubbles in liquids flowing inside microchannels. Lab Chip 13:365–376

Sutherland IW (2001) The biofilm matrix–an immobilized but dynamic microbial environment. Trends Microbiol 9:222–227

Svetličić V, Žutić V, Radić TM, Pletikapić G, Zimmermann AH, Urbani R (2011) Polymer networks produced by marine diatoms in the northern Adriatic Sea. Mar Drugs 9:666–679

Tam CK, Hyman WA (1973) Transverse motion of an elastic sphere in a shear field. J Fluid Mech 59:177–185

Whitfield C, Valvano MA (1993) Biosynthesis and expression of cell-surface polysaccharides in gram-negative bacteria. Adv Microb Physiol 35:135–246

Wingender J, Neu TR, Flemming H-C (1999) What are bacterial extracellular polymeric substances? Microbial extracellular polymeric substances. Springer, New York, pp 1–19

Wloka M, Rehage H, Flemming H-C, Wingender J (2004) Rheological properties of viscoelastic biofilm extracellular polymeric substances and comparison to the behavior of calcium alginate gels. Colloid Polym Sci 282:1067–1076

Xiao R, Zheng Y (2016) Overview of microalgal extracellular polymeric substances (EPS) and their applications. Biotechnol Adv 34:1225–1244

Zhang J (2015) Particle inertial focusing and separation in serpentine microchannels: mechanisms and applications. University of Wollongong, Wollongong, Australia

Zhou K, Hu Y, Zhang L, Yang K, Lin D (2016) The role of exopolymeric substances in the bioaccumulation and toxicity of Ag nanoparticles to algae. Sci Rep 6:32998